Computational Materials Science 152 (2018) 20–27

Contents lists available at ScienceDirect

Computational Materials Science

journal homepage: www.elsevier.com/locate/commatsci

Bandgap engineering of Janus MoSSe monolayer implemented by Se vacancy

Yan-Ni Wen[a,*], Ming-Gang Xia[b,c], Sheng-Li Zhang[c,*]

[a] Xi'an Aeronautical University, Shannxi 710077, People's Republic of China
[b] Department of Photoelectronic Information Science and Technology, School of Science, Xi'an Jiaotong University, Shaanxi 710049, People's Republic of China
[c] Department of Applied Physics, School of Science, Xi'an Jiaotong University, 710049, People's Republic of China

ARTICLE INFO

Keywords:
Janus MoSSe
Point vacancy
Linear vacancy
First-principles

ABSTRACT

Vacancy defects in 2D materials provide opportunities to tailor local physical, structural and electronic properties of point and linear vacancies in Janus MoSSe monolayers. In this paper, we studied vacancy formation in Janus MoSSe monolayers using ab initio density functional theory and observed that all vacancies are preferentially formed in the Se layer. In the case of point defects with more than two vacancies, a zigzag line feature is obtained for the lowest formation energy. In the case of infinite linear defects, the zigzag vacancy lines preferred to be distant from each other. The bandgap of a Janus MoSSe monolayer can be modulated by the concentration of vacancies. The bandgap energy decreased from 1.080 eV to 0.675 eV with the increase in the number of point vacancies. However, it is observed to oscillate around 0.530 eV with the increase of distance between the vacancy lines in the case of linear vacancies. This work is very useful in bandgap engineering of optical and electronic devices based on MoS_2.

1. Introduction

The study of two-dimensional (2D) monolayer materials has been a topic of interest since the first report of the successful fabrication of a 2D single layer graphene by Novoselov et al. in 2004 [1]. As a representative of 2D transition metal dichalcogenide (TMD), monolayer molybdenum disulfide (MoS_2) is proving to be a versatile material for a wide variety of applications due to its important role in lithium ion batteries (LIB) [2], flexible electronic devices [3], photoluminescence [4], valleytronics [5,6] and field effect transistors [7–9].

In order to create new physical functionalities, tremendous efforts have been directed towards breaking the out-of-plane mirror symmetry of the MoS_2 with electric fields [10,11]. Recently, Lu et al. reported a strategy to break the out-of-plane structural symmetry and grow a new structure, namely Janus MoSSe [12]. This structure was formed by replacing one S atom layer of MoS_2 monolayer with an Se layer, that resulted in a Mo atom layer sandwiched between S and Se atomic layers. This structural change is expected to bring about many interesting changes in its optical and electronic properties. At present, we only know its optical gap of 1.68 eV which close to the average of the optical gaps of MoS_2 and $MoSe_2$ [12].

It is well known that vacancy defects in 2D materials can be used to tailor the local physical properties. Examples include the generation of tunable magnetic phases in graphene and boron nitride with vacancies [13,14]. With different from graphene and boron nitride, some commonly vacancies observed in CVD grown monolayer MoS_2, including mono-sulfur vacancy (V_S), di-sulfur vacancy (V_{S2}) and rows formed by a number of sulfur vacancies [15,16]. These structures cannot produce magnetism in monolayer MoS_2 [17–20].

However, for the Janus MoSSe monolayer, we do not know whether a vacancy can cause a change in its physical properties. Thus we provide a systematic study of single and multiple vacancy formations in Janus MoSSe. From the results, we found that single and double Se vacancies next to each other have the lowest formation energies. As the number of vacancies increases, Se vacancies prefer to form zigzag lines unlike the vacancy rows in MoS_2. The lines prefer to exist at a large distance from each other. These defect structures cause variety of electronic band structures in a Janus MoSSe monolayer.

2. Computational methods

In this work, all calculations were performed using first-principles approaches based on the spin-polarized DFT within the projector augmented wave method, [21,22] as implemented in Vienna ab initio simulation package (VASP) [23]. The generalized gradient approximation (GGA) with the Perdew-Burke-Ernzerhof (PBE) functional was used

* Corresponding authors.
E-mail addresses: wenyanni353@sohu.com (Y.-N. Wen), zhangsl@mail.xjtu.edu.cn (S.-L. Zhang).

https://doi.org/10.1016/j.commatsci.2018.05.023
Received 24 February 2018; Received in revised form 27 April 2018; Accepted 14 May 2018
Available online 19 May 2018
0927-0256/

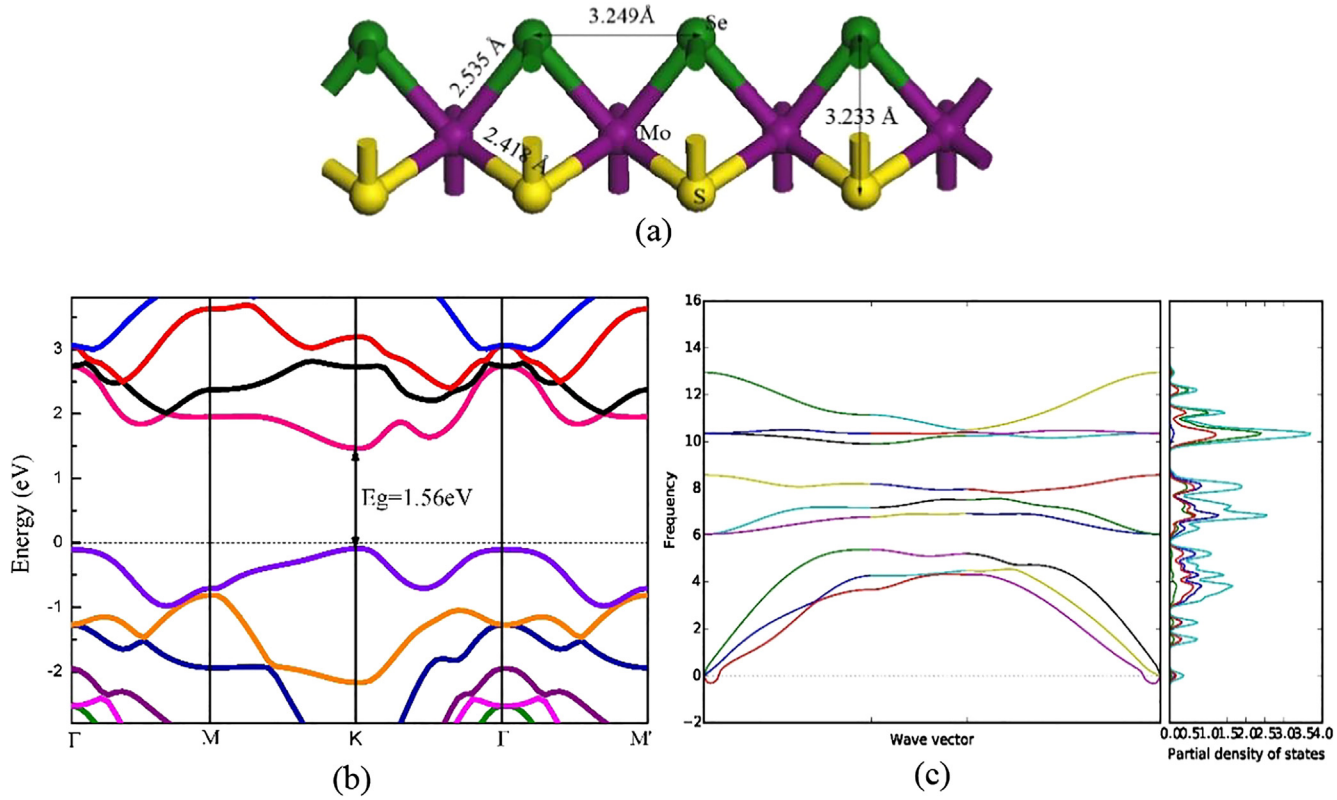

Fig. 1. (a) Atomic configurations of the optimized Janus MoSSe monolayer, (b) Electronic band structure and (c) Phonon spectrum of Janus monolayer MoSSe calculated at the optimized lattice constant of 3.249 Å.

to describe the electron exchange correlation interactions [24,25]. A periodic boundary condition is used to simulate 2D monolayer MoS_2, and all the structures are relaxed without any symmetry constraints. A vacuum space of 20 Å is used in periodic directions to avoid interactions between two neighboring images. The reciprocal space is represented by Monkhorst-Pack special k-point scheme [26] with 19 × 19 × 1 and 5 × 5 × 1 grid meshes for the 1 × 1 unit cell and the other supercells, respectively. The criteria of convergence for energy and force, as well as energy cutoff, are set to be 1×10^{-5} eV, 0.01 eV/Å, and 400 eV, respectively. This method has been previously applied to our calculations in previously reported works [27,28].

3. Results and discussion

3.1. Structure optimization of Janus MoSSe monolayer

The structure of Janus MoSSe monolayer was first optimized to obtain its lattice parameters. An optimized lattice constant a = 3.249 Å, S—Mo and Se—Mo bond lengths of 2.418 Å and 2.535 Å, respectively, and the nearest S—Se distance of 3.233 Å were all in accordance with previous results, as shown in Fig. 1(a) [12]. The calculated bandgap of 1.56 eV is in reasonable agreement with the theoretical prediction but lower than the experimental value of 1.68 eV, as shown in Fig. 1(b) [12]. The stability of the Janus MoSSe monolayer with the lattice constant a = 3.249 Å can be established by the phonon spectrum as shown in Fig. 1(c).

For comparison, the state-of-the-art hybrid functional (HSE06) is carried out to study the bandgap, and the value of 2.09 eV is obtained. HSE06 calculation over estimates the experimental bandgap value of 1.68 eV by 0.41 eV. However, PBE calculation only underestimates the bandgap by 0.12 eV. Hence, the bandgap from PBE in this paper is more accurate.

3.2. Structural and electronic properties of point vacancies

To understand the structural and electronic properties of point vacancies, 5 × 5 × 1 supercells were selected to construct various point vacancy structures. The formation energy can be obtained using the following equation:

$$E_f = E_V - E_{MoS_2} + \sum n_i \mu_i \quad (1)$$

where E_V and E_{MoS_2} are total energies of the defective and perfect 5 × 5 supercell in Janus MoSSe monolayer, respectively. n_i (i = S, Mo or Se) is the number of the removed i atom. μ_{Mo} is the per atom energy of the BCC (body-centered cube) Mo, μ_S and μ_{Se} are the per S and Se atom energies in MoS_2 and $MoSe_2$, respectively.

Three different single vacancies denoted by V_{Mo}, V_S and V_{Se} in Fig. 2, were constructed and then optimized. By using Eq. (1), the formation energies of 6.378 eV, 1.712 eV and 1.367 eV were obtained for V_{Mo}, V_S and V_{Se}, respectively. From the energy minimization, it is observed that V_{Se} is the most energetically stable vacancy in the Janus MoSSe monolayer.

After the formation of V_{Se}, a second vacancy is naturally formed in its immediate vicinity. From the V_{Se} in Fig. 2, three atoms of Mo, S and Se relocate in the immediate vicinity of V_{Se}. Thus, V_{SeMo}, V_{SeS} and V_{SeSe} were constructed and optimized, as shown in Fig. 2. By using Eq. (1), the formation energies of 4.423 eV, 1.521 eV and 1.252 eV can be obtained for V_{SeMo}, V_{SeS} and V_{SeSe}, respectively. From the energy minimization, V_{SeSe} is the most energetically favorable vacancy in the Janus MoSSe monolayer.

From Fig. 1(a), the bond length of Mo—Se (2.535 Å) is longer than that of Mo—S (2.418 Å). This results in a weaker interaction between Mo and Se as compared to Mo—S interaction. Thus, the most energetically stable mono- and di-vacancies (V_{Se} and V_{SeSe}) are all formed in the Se layer, as mentioned above. Given this observation, the third vacancy in the immediate vicinity of V_{SeSe} was constructed only in the

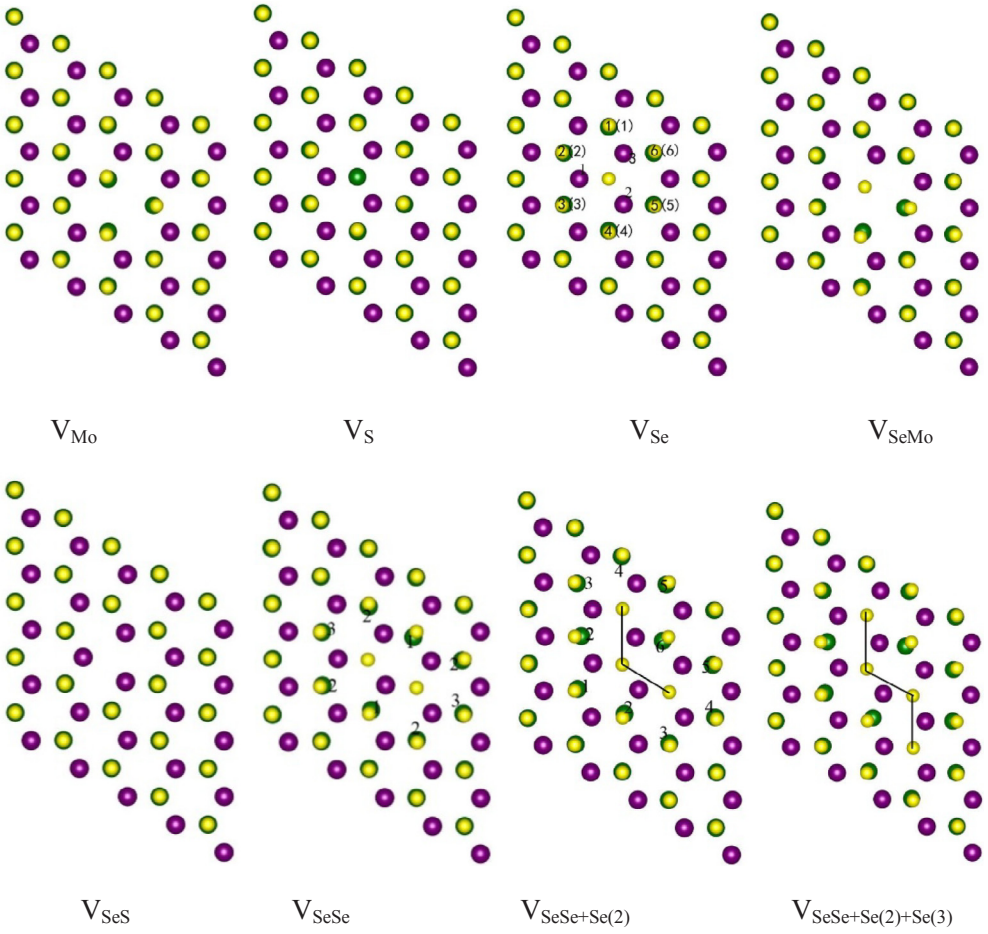

Fig. 2. Top views of the supercell models of the vacancy defects in Janus MoSSe monolayer. Green, yellow, and purple balls stand for lower Se, upper S, and middle Mo atoms, respectively. The black lines indicate the line of the multi-vacancy arrangement. (For interpretation of the references to color in this figure legend, the reader is referred to the web version of this article.)

Se atom layer.

Depending on the positional equivalence, three types of tri-vacancy cluster geometries are considered i.e. $V_{SeSe+Se(N)}$ (N:1, 2, 3), which is basically adding one vacancy to V_{SeSe} by removing an Se atom marked by 1, 2 or 3, as shown in Fig. 2. After optimization, the $V_{SeSe+Se(3)}$ structure was converted to $V_{SeSe+Se(2)}$. This indicates that three Se vacancies are mutually exclusive when they are positioned in a row. For $V_{SeSe+Se(2)}$ structure, the formation energy of 1.312 eV is lower than the one of 1.640 eV for $V_{SeSe+Se(1)}$. From the energy minimization, $V_{SeSe+Se(2)}$ is the most stable tri-vacancy in Janus MoSSe monolayer. Besides, the vacancy aggregation density of the $V_{SeSe+Se(2)}$ is less than that of $V_{SeSe+Se(1)}$. Thus, the most stable tri-vacancy also has the least vacancy aggregation density. In order to confirm these structural characteristics, the fourth vacancy in the immediate vicinity of $V_{SeSe+Se(2)}$ was constructed and studied in the following section.

For the fourth vacancy, six types of tetra-vacancy cluster geometries were considered i.e. $V_{SeSe+Se(2)+Se(M)}$, (M:1 to 6) which is basically adding one vacancy to $V_{SeSe+Se(2)}$ by removing the Se atom marked from 1 to 6, as shown in Fig. 2 $V_{SeSe+Se(2)}$. After optimization, the $V_{SeSe+Se(2)+Se(4)}$ structure converted to $V_{SeSe+Se(2)+Se(3)}$. This again indicates that the three Se vacancies are mutually exclusive when positioned in a row. By using Eq. (1), the formation energies of 2.004 eV, 1.582 eV, 1.508 eV, 1.380 eV and 1.333 eV are obtained for $V_{SeSe+Se(2)+Se(M)}$, M = 6, 2, 5, 1 and 3, respectively. Both the vacancy aggregation density and formation energy decrease in the following sequence of M = 6, 2, 5, 1 and 3. It is evident that in the Janus MoSSe monolayer the most stable tetra-vacancy structure is $V_{SeSe+Se(2)+Se(3)}$. In accordance with the above observations, the most stable vacancy structure has the least vacancy aggregation density. All of the vacancy formation energies are listed in Table 1.

Table 1
The calculated different vacancy formation energies E_f (eV) and the total energies E_V (eV) for the various vacancy defects of Janus MoSSe monolayer.

System	E_V (eV)	E_f (eV)
V_{Mo}	−499.903	6.378
V_S	−508.422	1.712
V_{Se}	−509.519	1.367
V_{SeMo}	−499.903	4.423
V_{SeS}	−508.422	1.521
V_{SeSe}	−509.519	1.252
$V_{SeSe+Se(1)}$	−503.380	1.640
$V_{SeSe+Se(2)}$	−503.708	1.312
$V_{SeSe+Se(2)+Se(1)}$	−497.829	1.380
$V_{SeSe+Se(2)+Se(2)}$	−497.627	1.582
$V_{SeSe+Se(2)+Se(3)}$	−497.876	1.333
$V_{SeSe+Se(2)+Se(5)}$	−497.701	1.508
$V_{SeSe+Se(2)+Se(6)}$	−497.205	2.004

The difference charge densities of the most stable mono-, di-, tri- and tetra-vacancies structures, namely V_{Se}, V_{SeSe}, $V_{SeSe+Se(2)}$ and $V_{SeSe+Se(2)+Se(3)}$, respectively, are shown in Fig. 3. It can be seen that the highest charge depletion and accumulation occurs on the Se vacancies and the top S atoms corresponding to the Se vacancy, respectively. The charges on the Se atoms near the vacancy are found to shift to the vacancy. A higher charge transfer occurs on the Se atoms between two vacancies than the others.

The electronic band structure of perfect 5 × 5 Janus monolayer MoSSe and the ones with V_{Se}, V_{SeSe}, $V_{SeSe+Se(2)}$ and $V_{SeSe+Se(2)+Se(3)}$ vacancies are shown in Fig. 4. From the calculation results, the bandgaps of 1.080 eV, 0.874 eV, 0.765 eV and 0.675 eV are obtained for V_{1Se}, V_{2SeII}, V_{3SeIII} and V_{4SeIV}, respectively. In the case of the material

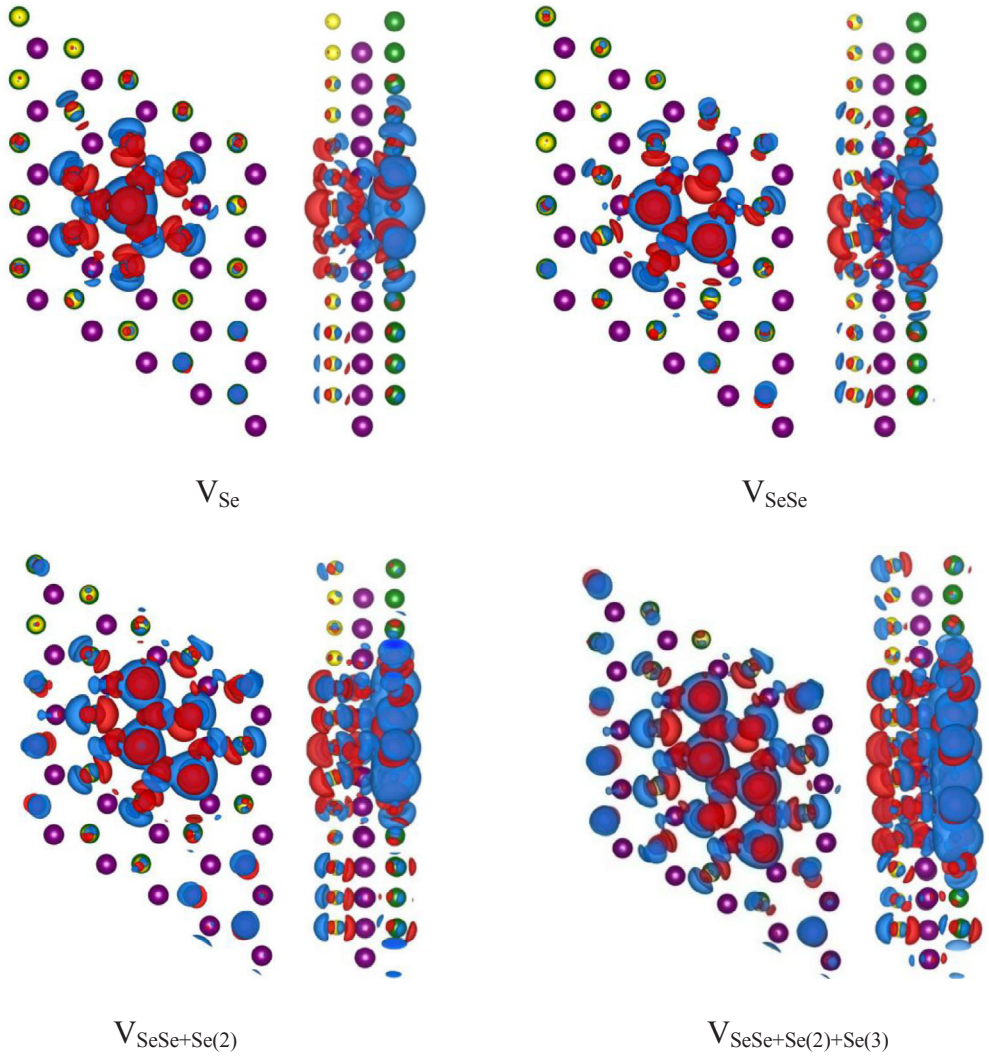

Fig. 3. Difference charge densities for the V_{Se}, V_{SeSe}, $V_{SeSe+Se(2)}$ and $V_{SeSe+Se(2)+Se(3)}$. The left and right structures were respectively the top and side views of the supercell. The red and blue colors represent the charge accumulation and depletion, respectively, and the isosurface level was set to 0.02 e/Å^3. (For interpretation of the references to color in this figure legend, the reader is referred to the web version of this article.)

with defects, it retains its semiconductor property to the pristine state. One of the differences when compared with the perfect material is that the highest point of the valence band is the Γ point. Additionally, some flat or quasi flat belts appear between the Fermi level and conduction band. Each vacancy corresponds to two quasi flat belts. This is due to the fact that with the increase of vacancy number, the quasi flat band doubles, and the conduction bands diffusion toward the Fermi surface. Simultaneously, the dispersion of quasi flat belts is enhanced and the bottom of the quasi flat belts gradually migrates from K point to Γ point. This results in the decrease of the bandgap when the number of vacancies increases.

In order to further understand the mechanism of flat belt production, the total density of states (TDOS) for all the Se, S and Mo atoms in the 5 × 5 supercell with V_{Se} and for all the Se, S and Mo atoms around the Se single vacancy, was determined (Fig. 5). From Fig. 5, it is evident that the main charge contribution of the quasi flat belt is from Mo atoms around the Se single vacancy. This indicates that the vacancy is a local state and this feature is applicable to other vacancies as well.

By observing the most stable structures of the tri- and tetra-vacancy structures, it is found that more Se vacancies tend to line up along the zigzag lines. These lines have the lowest vacancy aggregation density in all their corresponding optimized vacancy structures. In order to further confirm this fact, the same vacancy cluster geometries were constructed and calculated in the 6 × 6 supercells. The results were in agreement with the earlier observations. Thus, it is speculated that the zigzag line can be extended indefinitely when the vacancies continue to increase in the two-dimensional monolayer MoSSe. However, it is important to know if the addition of more vacancies would decrease the distance between the zigzag lines. To probe this, the structural and electronic properties of Se zigzag linear vacancy in Janus MoSSe monolayer were studied as discussed in the next section.

3.3. Structural and electronic properties of zigzag linear vacancy

The supper lattice of the vacancy line can be constructed by moving two Se atoms in the (X, Y) repetitive computational cell, where X and Y indicate the number of the Mo−S chains along *x* and *y* directions, respectively, as shown in Fig. 6. The optimization schematic diagrams of Se Zigzag linear vacancy in the 2 × 2 (3, 2) computational cells of Janus MoSSe monolayer are also shown in Fig. 6. However, a larger X implies a larger distance between the vacancy lines. In order to simplify the study, the repetitive computational cells (3, 2), (4, 2), (5, 2), (6, 2) and (7, 2) are studied, where X = 3, 4, 5, 6 and 7 and Y = 2.

Firstly, the repetitive computational cells (3, 2), (4, 2), (5, 2), (6, 2) and (7, 2) with Se Zigzag linear vacancy were optimized. Wrinkles were found in each computational cell, as is evident from the side views of

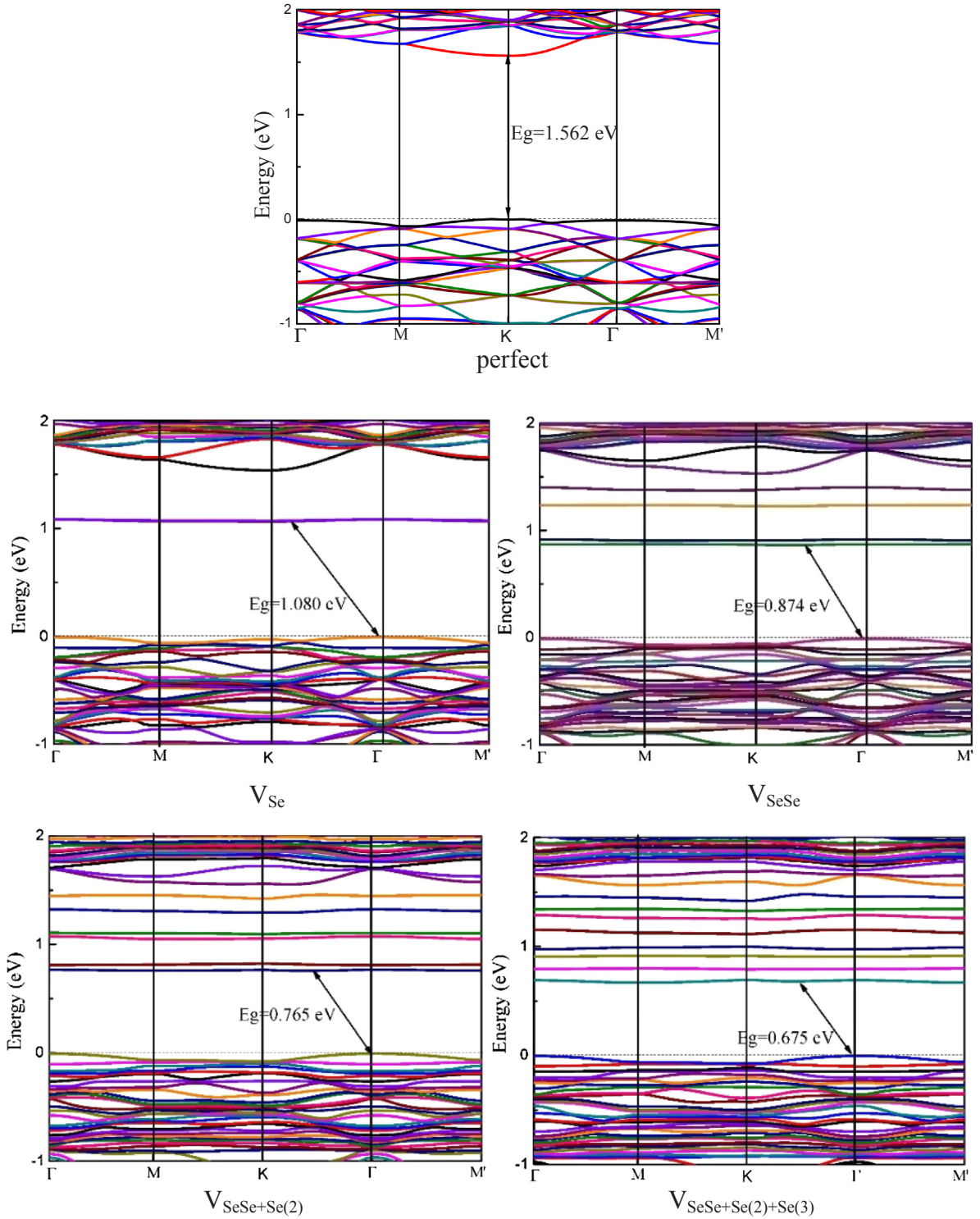

Fig. 4. Electronic band structure of perfect 5 × 5 Janus monolayer MoSSe and the ones with V_{Se}, V_{SeSe}, $V_{SeSe+Se(2)}$ and $V_{SeSe+Se(2)+Se(3)}$, respectively.

the 2 × 2 (3, 2) repetitive computational cells in Fig. 6. The degree of wrinkle was defined using the distance from the top S atom and the bottom Se atom minus their original distance 3.233 Å, and then dividing by the width of the repetitive computational cell along *x* direction. Fig. 7 shows the variation of the wrinkle degree as a function of X. The curve resembles a section of a downward parabola. This indicates the wrinkle degree increases with the increase of the X within the scope of our study.

Secondly, the average formation energy of one vacancy was calculated by using Eq. (1) in each repetitive computational cell. The values of 1.505 eV, 1.322 eV, 1.242 eV, 1.184 eV and 1.139 eV were obtained for Se zigzag linear vacancy in (3, 2), (4, 2), (5, 2), (6, 2) and (7, 2) repetitive computational cell, respectively. The vacancy formation energy decreased with the increase in X in the repetitive computational cell, which has an opposite tendency when compared with the degree of wrinkle (Fig. 7). Thus, the zigzag vacancy lines prefer to be distant from each other. However, the tendency for zigzag linear vacancy leads to a greater degree of wrinkle formation.

Fig. 8 shows the difference charge densities for the zigzag linear vacancy in (3, 2), (4, 2), (5, 2), (6, 2) and (7, 2) computational cells,

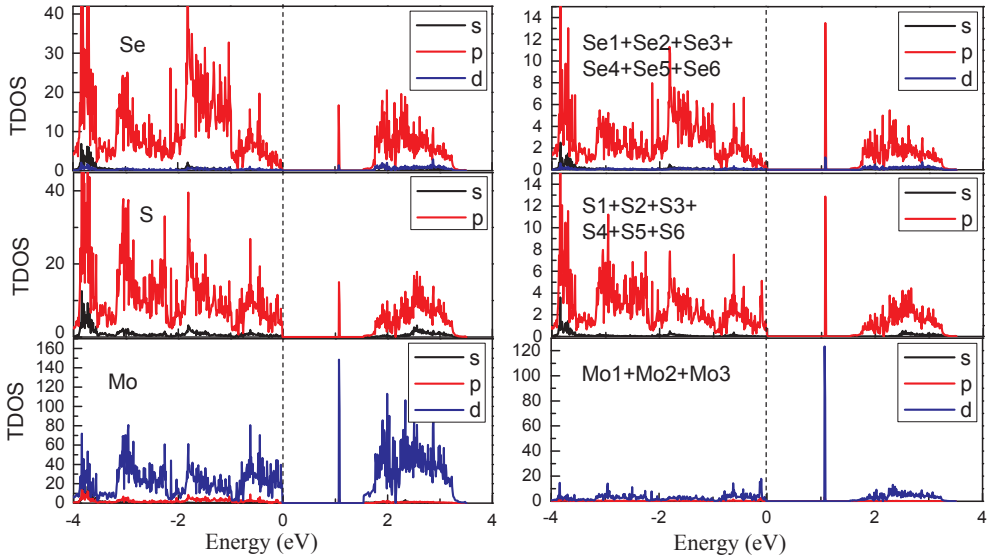

Fig. 5. Total density of states (TDOS) for the Se, S and Mo atoms in the 5 × 5 Janus monolayer MoSSe supercell with V_{Se} and the ones summed all the Se atoms (marked from 1 to 6 in the parentheses), S atoms (marked from 1 to 6) and Mo atoms (marked from 1 to 3) around the Se single vacancy, as shown in Fig. 2 V_{Se}.

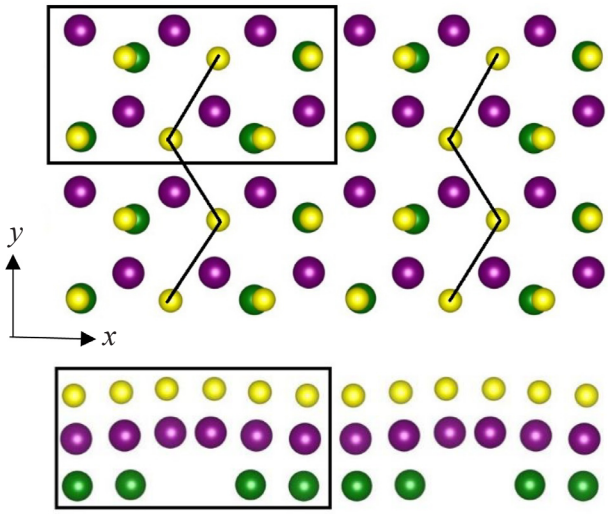

Fig. 6. The optimization schematic diagrams of Se Zigzag linear vacancy in the 2 × 2 (3, 2) (in the black box) repetitive computational cells of Janus MoSSe monolayer. Green, yellow, and purple balls stand for lower Se, upper S, and middle Mo atoms, respectively. The black lines indicate the Zigzag linear vacancy arrangement. The structures above and below are respectively the top and side views of the 2 × 2 (3, 2) computational cells. (For interpretation of the references to color in this figure legend, the reader is referred to the web version of this article.)

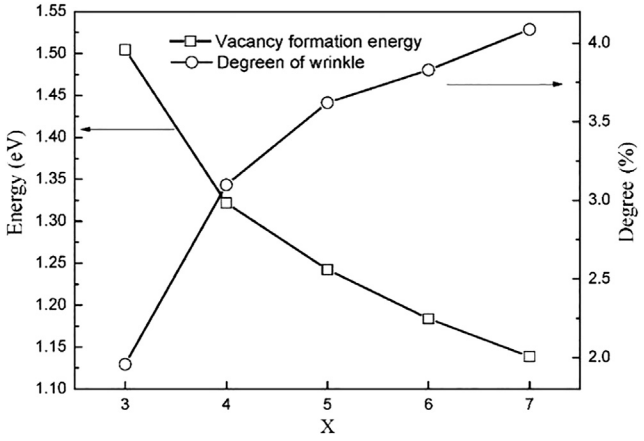

Fig. 7. The degree of wrinkle degree and the average vacancy formation energies as a function of X.

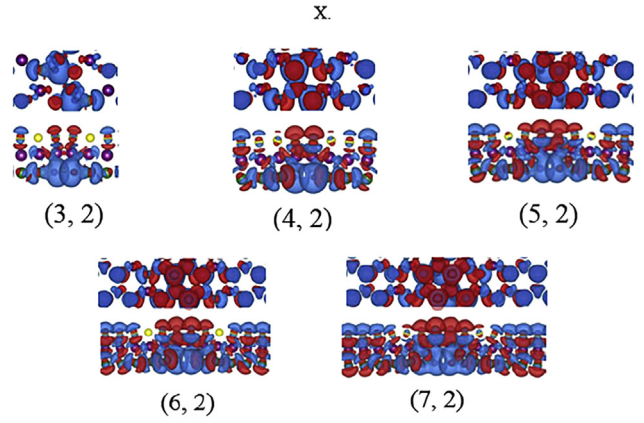

Fig. 8. Difference charge densities for the zigzag linear vacancy in (3, 2), (4, 2), (5, 2), (6, 2) and (7, 2) repetitive computational cell, respectively. The top and down structures were respectively the top and side views of the supercell. The red and blue colors represented the charge accumulation and depletion, respectively, and the isosurface level was set to 0.02 e/Å^3. (For interpretation of the references to color in this figure legend, the reader is referred to the web version of this article.)

respectively. It is clear that the highest charge depletion and accumulation is found on the Se vacancies and the top S atoms corresponding to the Se vacancy, respectively. The charges on the Se atoms near the vacancy tend to shift to the vacancy. This phenomenon is similar to the one seen in the case of point defects. When S and Se atoms are far away from the vacancy, the charges are transferred from the top (S layer) to the bottom (Se layer).

Fig. 9 show the electronic band structures of Janus monolayer MoSSe with zigzag linear vacancy in (3, 2), (4, 2), (5, 2), (6, 2) and (7, 2) repetitive computational cell. The bandgaps of 0.583 eV, 0.523 eV, 0.557 eV, 0.538 eV and 0.529 eV were obtained for (3, 2), (4, 2), (5, 2), (6, 2) and (7, 2) computational cell, respectively. The bandgaps oscillated around 0.530 eV following the X (X > 3) of the computational cell. The greatest and indirect bandgap of 0.583 eV appears in the X = 3

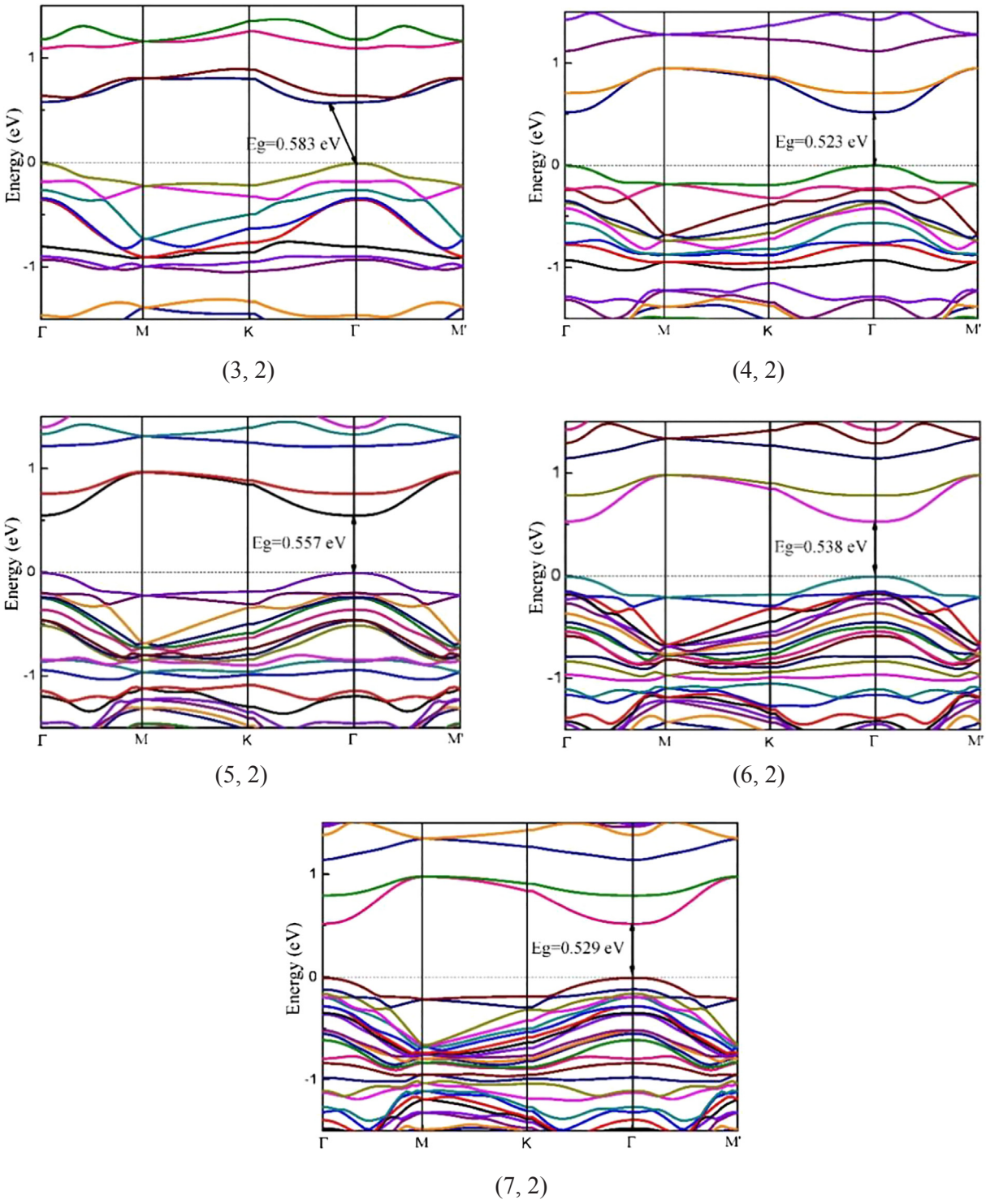

Fig. 9. Electronic band structures of Janus monolayer MoSSe with zigzag linear vacancy in (3, 2), (4, 2), (5, 2), (6, 2) and (7, 2) repetitive computational cell, respectively.

computational cell due to the interaction between the vacancy lines. When the computational cell X > 3, the bandgaps are direct in the Γ point.

4. Conclusion

The structural and electronic properties of point and linear vacancy in the Janus MoSSe monolayer were studied by the ab initio density functional theory. The Janus monolayer MoSSe was optimized by PBE and a lattice constant of 3.249 Å was obtained. The phonon spectrum was evaluated and the structural stability was established. The structural and electronic properties of different number of point vacancies were also studied. Point vacancies preferred to form in the Se layer of Janus MoSSe monolayer due to the weaker interaction between Mo and Se as compared to the Mo-S interaction. V_{Se} and V_{SeSe} constituted the defects corresponding to the lowest energy configurations for the mono- and di-vacancies, respectively. Depending on the number of the Se vacancy, they are preferred to line up along the zigzag lines in the Se

layer. This linear arrangement facilitated more vacancies and had the lowest vacancies aggregation density. Indirect bandgaps were observed for all point defective Janus MoSSe monolayers and the bandgap energies decreased with the increase of vacancy number. Finally, the structural and electronic properties of zigzag linear vacancy were studied where a wrinkle feature was observed. The degree of wrinkle was found to increase with an increase in X. Then the average formation energy of one vacancy was calculated and found follow an opposite trend as compared to the wrinkle degree. Thus, the zigzag vacancy lines preferred to be distant from each other and the degree of wrinkle was greater if the zigzag linear vacancy was easily formed. All of the electronic band structures of linear defective Janus MoSSe monolayer are direct except the one in (3, 2) repetitive computational cell. The bandgaps oscillated around 0.530 eV following the X (X > 3) of the (X, 2) computational cell. The largest bandgap was obtained for the (3, 2) repetitive computational cell and had a magnitude of 0.583 eV.

Acknowledgements

This work was supported by the National Natural Science Foundation (NSF) of China (Grants Nos. 11774278, 10704059, 11774280, and 11374237), Shannxi Postdoctoral Sustentation Fund, China (2016BSHEDZZ78), the Fundamental Research Funds for Central Universities (2012jdgz04) and the Scientific Research Foundation for the Returned Overseas Chinese Scholars, State Education Ministry (2013) for financial support.

References

[1] K.S. Novoselov, A.K. Geim, S.V. Morozov, D. Jiang, Y. Zhang, S.V. Dubonos, I.V. Grigorieva, A.A. Filrsov, Electric field effect in atomically thin carbon films, Science 306 (2004) 666.
[2] H. Wang, H. Kim, J. Cho, MoS_2 nanoplates consisting of disordered graphene-like layers for high rate lithium battery anode materials, Nano Lett. 11 (2011) 4826.
[3] S. Bertolazzi, J. Brivio, A. Kis, Stretching and breaking of ultrathin MoS_2, ACS Nano 5 (2011) 9703.
[4] G. Eda, H. Yamaguchi, D. Voiry, T. Fujita, M. Chen, M. Chhowalla, Photo luminescence from Chemically Exfoliated MoS_2, Nano Lett. 11 (2012) 5111.
[5] Y. Shimazaki, M. Yamamoto, I.V. Borzenets, K. Watanabe, T. Taniguchi, S. Tarucha, Generation and detection of pure valley current byelectrically induced Berry curvature in bilayer grapheme, Nat. Phys. 11 (2015) 1032.
[6] T. Cao, G. Wang, W. Han, H. Ye, C. Zhu, J. Shi, Q. Niu, P. Tan, E. Wang, B. Liu, J. Feng, Valley-selective circular dichroism of monolayer molybdenum disulphide, Nat. Commun. 3 (2012) 887.
[7] M. Fuhrer, J. Hone, Measurement of mobility in dual-gated MoS_2 transistors, Nat. Nanotechnol. 8 (2013) 146.
[8] W. Wu, D. De, S.C. Chang, Y.N. Wang, H.B. Peng, J.M. Bao, S.S. Pei, High mobility and high on/off ratio field-effect transistors based on chemical vapor deposited single-crystal MoS_2 grains, Appl. Phys. Lett. 102 (2013) 142106.
[9] D. Jariwala, V.K. Sangwan, D.J. Late, J.E. Johns, V.P. Dravid, T.J. Marks, L.J. Lauhon, M.C. Hersam, Band-like transport in high mobility unencapsulated single-layer MoS_2 transistors, Appl. Phys. Lett. 102 (2013) 173107.
[10] H. Yuan, M.S. Bahramy, K. Morimoto, S. Wu, K. Nomura, B. Yang, H. Shimotani, R. Suzuki, M. Toh, C. Kloc, X. Xu, R. Arita, N. Nagaosa, Y. Iwasa, Zeeman-type spin splitting controlled by an electric field, Nat. Phys. 9 (2013) 563.
[11] S. Wu, J.S. Ross, G.B. Liu, G. Aivazian, A. Jones, Z. Fei, W. Zhu, D. Xiao, W. Yao, D. Cobden, X. Xu, Electrical tuning of valley magnetic moment through symmetry control in bilayer MoS_2, Nat. Phys. 9 (2013) 149.
[12] A.Y. Lu, H. Zhu, J. Xiao, C.P. Chuu, Y. Han, M.H. Chiu, C.C. Cheng, C.W. Yang, K.H. Wei, Y. Yang, Y. Wang, D. Sokaras, D. Nordlund, P. Yang, D.A. Muller, M.Y. Chou, X. Zhang, L.J. Li, Janus monolayers of transition metal dichalcogenides, Nat. Nanotechnol. 12 (2017) 744.
[13] J.H. Chen, L. Li, W.G. Cullen, E.D. Williams, M.S. Fuhrer, Tunable kondo effect in graphene with defects, Nat. Phys. 7 (2011) 535.
[14] B. Ouyang, J. Song, Strain engineering of magnetic states of vacancy-decorated hexagonal boron nitride, Appl. Phys. Lett. 103 (2013) 102401.
[15] D. Le, T.B. Rawal, T.S. Rahman, Single-layer MoS_2 with sulfur vacancies: structure and catalytic application, J. Phys. Chem. C 118 (2014) 5346.
[16] H.P. Koms, S. Kurasch, O. Lehtinen, U. Kaiser, A.V. Krasheninnikov, From point to extended defects in two-dimensional MoS_2: evolution of atomic structure under electron irradiation, Phys. Rev. B 88 (2013) 035301.
[17] W. Zhou, X.L. Zou, S. Najmaei, Z. Liu, Y.M. Shi, J. Kong, J. Lou, P.M. Ajayan, B.I. Yakobson, J.C. Idrobo, Intrinsic structural defects in monolayer molybdenum disulfide, Nano Lett. 13 (2013) 2615.
[18] Y.G. Zhou, P. Yang, H.Y. Zu, F. Gao, X.T. Zu, Electronic structures and magnetic properties of MoS_2 nanostructures: atomic defects, nanoholes, nanodots and antidots, Phys. Chem. Chem. Phys. 15 (2013) 10385.
[19] Y.C. Cheng, Z.Y. Zhu, W.B. Mi, Z.B. Guo, U. SchwingenschlÖgl, Prediction of two-dimensional diluted magnetic semiconductors: doped monolayer MoS_2 systems, Phys. Rev. B 87 (2013) 100401.
[20] D. Liu, Y. Guo, L. Fang, J. Robertson, Sulfur vacancies in monolayer MoS_2 and its electrical contacts, Appl. Phys. Lett. 103 (2013) 183113.
[21] J.P. Perdew, K. Burke, M. Ernzerhof, Generalized gradient approximation made simple, Phys. Rev. Lett. 77 (1996) 3865.
[22] G. Kresse, D. Joubert, From ultrasoft pseudopotentials to the projector augmented-wave method, Phys. Rev. B 59 (1999) 1758.
[23] G. Kresse, J. Furthmüller, Efficient iterative schemes for ab-inition total-energy calculations using a plane-wave basis set, Phys. Rev. B 54 (1996) 11169.
[24] P. Hohenberg, W. Kohn, In homogeneous electron gas, Phys. Rev. B 136 (1964) 864.
[25] P.E. Blöchl, Projector augmented-wave method, Phys. Rev. B 50 (1994) 17953.
[26] H.J. Monkhorst, J.D. Pack, Special points for brillouin-zone integrations, Phys. Rev. B 13 (1976) 5188.
[27] Y.N. Wen, M.G. Xia, S.L. Zhang, Size effect on the magnetic and electronic properties of the monolayer lateral hetero-junction WS_2-MoS_2 nanoribbon, Appl. Surf. Sci. 371 (2016) 376.
[28] Y.N. Wen, P.F. Gao, X. Chen, M.G. Xia, Y. Zhang, S.L. Zhang, Width-dependent structural stability and magnetic properties of monolayer zigzag MoS_2 nanoribbons, Mod. Phys. Lett. B 31 (2017) 1750017.